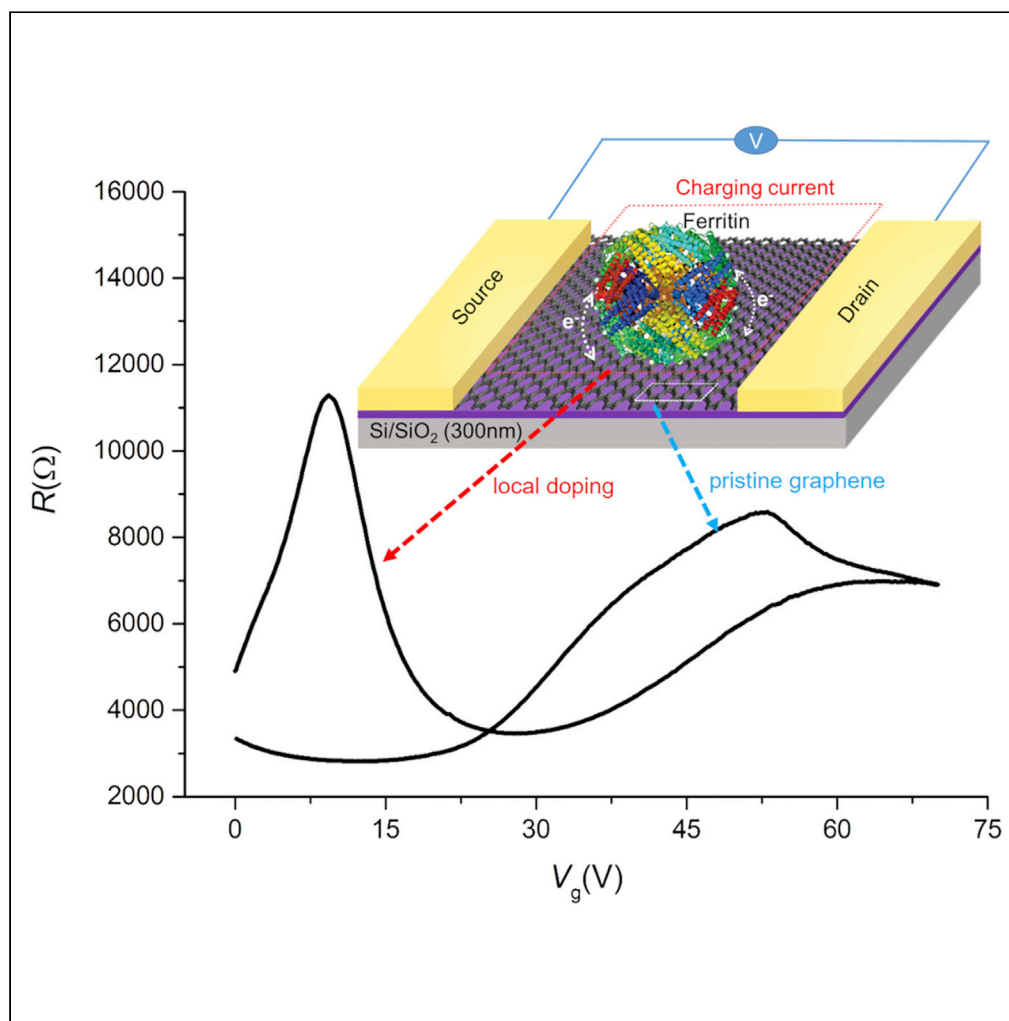


Article

Biomolecular control over local gating in bilayer graphene induced by ferritin



Senthil Kumar
Karuppannan,
Jens Martin,
Wentao Xu, Rupali
Reddy Pasula,
Sierin Lim,
Christian A.
Nijhuis

jens.martin@ikz-berlin.de
(J.M.)
c.a.nijhuis@utwente.nl (C.A.N.)

Highlights

Local gating with 12 nm
resolution by charge
trapping in ferritin.

Adsorption of ferritin on
graphene via non-invasive
self-assembly.

Charging controlled via
iron oxide loading of
ferritin.

Visualization of individual
ferritins on graphene by
atomic force microscopy.

Karuppannan et al., iScience
25, 104128
April 15, 2022 © 2022 The
Author(s).
[https://doi.org/10.1016/
j.isci.2022.104128](https://doi.org/10.1016/j.isci.2022.104128)

Article

Biomolecular control over local gating in bilayer graphene induced by ferritin

Senthil Kumar Karuppanan,¹ Jens Martin,^{2,3,6,*} Wentao Xu,² Rupali Reddy Pasula,⁴ Sierin Lim,⁴ and Christian A. Nijhuis^{1,2,5,7,*}

SUMMARY

Electrical field-induced charge modulation in graphene-based devices at the nanoscale with ultrahigh density carrier accumulation is important for various practical applications. In bilayer graphene (BLG), inversion symmetry can simply be broken by an external electric field. However, control over charge carrier density at the nanometer scale is a challenging task. We demonstrate local gating of BLG in the nanometer range by adsorption of AfFtnAA (which is a bioengineered ferritin, an iron-storing globular protein with $\varnothing = 12$ nm). Low-temperature electrical transport measurements with field-effect transistors with these AfFtnAA/BLG surfaces show hysteresis with two Dirac peaks. One peak at a gate voltage $V_{BG} = 35$ V is associated with pristine BLG, while the second peak at $V_{BG} = 5$ V results from local doping by ferritin. This charge trapping at the biomolecular length scale offers a straightforward and non-destructive method to alter the local electronic structure of BLG.

INTRODUCTION

Controlling the charge carrier density at small dimensions is a major challenge in nano-electronics in which 2D materials can play a crucial role (Trauzettel et al., 2007; Fehske et al., 2015; Tran and Mulchandani, 2016). For instance, locally gated graphene allows us to study interesting phenomena such as Klein tunneling (Katsnelson et al., 2006; Young and Kim, 2009; Logemann et al., 2015; Oh et al., 2016; Solnyshkov et al., 2016), whispering gallery modes (Zhao et al., 2015), and graphene super-lattices (Dubey et al., 2013; Gorbachev et al., 2014; Krishna Kumar et al., 2017). These phenomena are directly related to quantum interference of relativistic charge carriers. However, to experimentally observe quantum interference phenomena, the mean free path must be longer than the locally gated regions. Beyond local gating, there is interest in local confinement to enable tunable quantum dots and ballistic 1D channels. In principle, it is possible to create a bandgap in graphene by lateral confinement or breaking of sub-lattice symmetry using an external electric field, in particular, in Bernal-stacked bilayer graphene, inversion symmetry can simply be broken by an external electric field (Overweg et al., 2018). Even in clean systems, this requires very small length scales (260–100 nm) for devices (Allen et al., 2012; Solnyshkov et al., 2016). In practice, however, nanofabrication approaches are difficult to implement, and the observation of charge confinement of Dirac electrons in nanostructured graphene has proven surprisingly challenging. Hence, controlled electrostatic gating on the nanometer scale through molecule-graphene interaction offers an interesting approach.

Local potential modulation can be introduced by various means including electrostatic or chemical gating which is achieved through chemical doping with adsorption of charged molecules as a dopant (Dong et al., 2009; Farmer et al., 2009; Kulkarni et al., 2016; Mulyana et al., 2016a), or high-resolution resist materials like hydrogen silsesquioxane (HSQ) (Brenner and Murali, 2010) and SU8 (Yun et al., 2014), as a complementary dopant, or by constructing double gates below and on top of the graphene layer through electrostatic modification of gate insulator (Chiu et al., 2010) or by focused laser irradiation (Kim et al., 2013; Seo et al., 2014), or strain of graphene to induce electrostatic gating, (Sun et al., 2016) and as there had been several examples in the STM community (i.e., Crommie group) (Velasco et al., 2018). A major challenge is to control charge carrier density at the true nanometer scale (Kong et al., 2014; Solís-Fernández et al., 2016). Typical lithography techniques only allow patterning down to about 10 nm (Mojarad et al., 2015; Winter et al., 2019). On the other hand, the natural length scale of molecules lies in the 1.0 nm range. Hence, gating through molecular entities could play a significant role in future nano-electronics (Park et al., 2012; Samuels and Carey, 2013). However, control over adsorption, distribution, and charge transfer of the molecules is a challenging task, even more so on graphene with its chemically inert p-orbitals at the surface.

¹Department of Chemistry, National University of Singapore, 3 Science Drive 3, Singapore 117543, Singapore

²Centre for Advanced 2D Materials and Graphene Research Centre, National University of Singapore, 6 Science Drive 2, Singapore 117546, Singapore

³Department of Physics, National University of Singapore, 3 Science Drive 3, Singapore 117543, Singapore

⁴School of Chemical and Biomedical Engineering, Nanyang Technological University, 70 Nanyang Drive, Singapore 637457, Singapore

⁵Hybrid Materials for Opto-Electronics Group, Department of Molecules and Materials, MESA+ Institute for Nanotechnology and Center for Brain-Inspired Nano Systems, Faculty of Science and Technology, University of Twente, P.O. Box 217, 7500 AE Enschede, the Netherlands

⁶Present address: Leibniz Institut für Kristallzüchtung Max-Born-Strasse 2, 12489 Berlin, Germany

⁷Lead contact

*Correspondence: jens.martin@ikz-berlin.de (J.M.), c.a.nijhuis@utwente.nl (C.A.N.)

<https://doi.org/10.1016/j.isci.2022.104128>



In general, two common approaches have been used to locally tune the electrical properties of graphene. i) Chemical functionalization of graphene by replacing carbon atoms within the graphene lattice by nitrogen or boron, which causes a shift in the work function, but it also disorders the graphene lattice in an uncontrollable manner (Vicarelli et al., 2015). ii) Adsorption of molecules onto graphene via physisorption (non-covalent interactions) using ionic (Kulkarni et al., 2016; Song et al., 2016; Sun et al., 2016) or aromatic anchoring groups (Macleod and Rosei, 2014; Lin et al., 2015). In both methods, the distribution of the adsorbates is often inhomogeneous, resulting in uncontrolled doping, carrier density variations, and degraded carrier mobility. The (supra)molecular and electronic structure of molecular assemblies on solid surfaces is determined by various factors, such as surface substrate interactions, molecule-molecule interactions, or the properties of the solvent from which the molecule was deposited from (Yang and Wang, 2009; Macleod and Rosei, 2014). To locally gate graphene via molecular adsorbates, it is, in principle, important to control the orientation and packing of the molecule and the associated charge transfer between the molecule and the graphene (Yang and Wang, 2009; Xiao et al., 2013). It has been proposed to control the orientation of molecules on the surface by applying electric/magnetic fields or by nanomechanical symmetry breaking effects using the tip of an atomic force microscope (Yuan et al., 2008; Hong et al., 2018), but forming and controlling well-defined molecular domains remains challenging.

In the past few years, electronic circuits have been demonstrated using graphene-based field effect transistors (FETs); however, depending on the graphene-dielectric interface and the testing conditions (air ambient versus vacuum), the graphene-based FET often exhibits hysteresis, which is primarily caused by charge trapping at the graphene-dielectric interfaces, charge creep, and by ambient molecules (i.e., water and oxygen) in contact with the graphene surface (Joshi et al., 2010). The charge trapping can be reduced or removed by measurements carried out under vacuum conditions or at low temperatures after a vacuum annealing step (Lohmann et al., 2009; Wang et al., 2010). However, trapping at the interface is a challenging problem because it compromises device reliability and operation issues that translate to changes in the measured carrier concentrations and contact resistance.

Here, we demonstrate local gating of charge carriers in bilayer graphene (BLG) incorporated in FET configuration induced by surface adsorption of biomolecules, archaeal ferritin AfFtn obtained from *Archaeoglobus fulgidus* (we used a modified AfFtn where two amino acids (K150 and R151) are substituted with alanines resulting in closed-pore structure, AfFtnAA (Sana et al., 2013)). Ferritins are highly symmetrical proteins of globular, cage-like structure with a 12 nm outer, and 8 nm inner, diameter. The biological function of ferritin is to store Fe ions in the hollow interior and release the Fe ions on demand. The iron ions are stored in the form of ferrihydrite nanoparticles, and loading can be controlled from 500 Fe ions atoms/cage to 4800 Fe ions/cage; these ferritin are remarkably stable up to 80 °C and a wide range of pH values (pH = 2.0–10.0). Watt et al. demonstrated nano-energy storage systems based on ferritins with iron oxide nanoparticles and reported that the coulomb capacity of this ferritin-based energy storage device was ~1400 times higher than that of vesicle battery where each ferritin can accommodate a charge of 5×10^{-16} coulombs (~3600 electrons) (Watt et al., 2012). We measured the resistance of BLG-based FET with a different surface coverage of ferritin as a function of applied gate voltage. We found that physisorbed ferritin induces significant local electron/hole doping of 79 ± 23 electrons for ferritin with iron oxide nanoparticles (NPs) and 65 ± 7 holes for apoferritin, corresponding to charge carrier densities of 10^{14} cm^{-2} comparable with ionic gating (Yuan et al., 2009). We attribute this effect to formation of dense monolayers of ferritin molecule on the graphene surface (Qiu et al., 2013; San et al., 2014) combined with the high charge storage capacity of ferritin. Because of the single-sided deposition of the molecules (ferritin adsorbed on top-surface of BLG), the resulting electric field also opens up a bandgap in a non-destructive way.

RESULTS AND DISCUSSION

Figure 1 shows the schematic illustration of our FETs with BLG in SiO₂/Si (which serves as the back gate electrode) and connected with 2 Au electrodes. Onto the BLG, ferritin was adsorbed. The detailed procedure for device fabrication and ferritin adsorption on graphene is given in STAR Methods. Briefly, the BLG (obtained by mechanical exfoliation with the standard scotch tape method) was deposited on highly doped Si-p⁺/SiO₂. The electrodes (Ti/Au of 5/60 nm) were patterned using e-beam lithography and deposited by thermal evaporation. After the fabrication of metal contacts, the device was vacuum annealed at 200 °C for 2 h to remove the physisorbed organic contaminants from the BLG surface. The contact resistance between the BLG and Ti/Au interface changed from 243 Ω/μm to 350 Ω/μm after adsorption of a dense monolayer of ferritin (see STAR Methods and Supplemental information); these contact resistances are consistent with previously

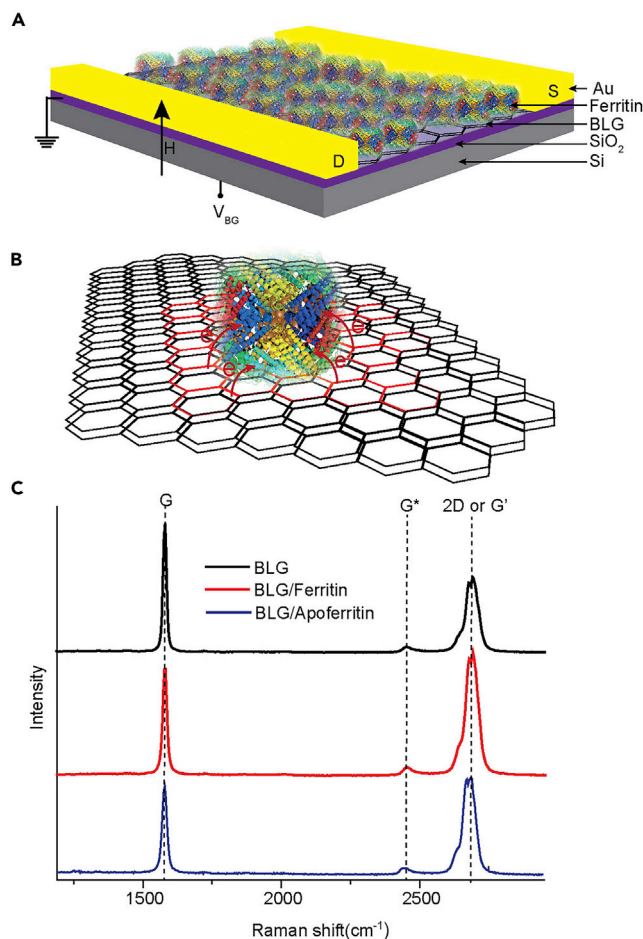


Figure 1. Device concept and biomolecule-induced local charging

(A) Schematic illustration of the BLG-FET device with AfFtnAA (Fe3600 loading/cage) on bilayer graphene BLG with channel width = 4.5 μm and length = 3.1 μm .

(B) Schematic illustration of the electrostatic interaction between BLG and charged ferritin. The ferritin extracts charge from a limited area leading to charge accumulation and opens up bandgap in BLG.

(C) Raman spectra of BLG before and after adsorption of dense monolayer of AfFtnAA and apo-AfFtnAA.

reported contact resistances between BLG and Ti/Au contacts (Liu et al., 2013). We also immersed different devices into aqueous solutions of ferritin (1 mg/L) with variable amounts of times (30–120 min) to control the surface coverage. The ferritins adsorb via physisorption likely mediated by graphene-NH₂ interactions. We have shown previously that alkyl-amines readily adsorb on graphene to yield stable SAMs (Song et al., 2016), hence free NH₂ present at the external surface of ferritin can readily interact with graphene resulting in stable assemblies. As a control, we also prepared a device with apoferritin (apo-AfFtnAA).

We measured the Raman spectra of the ferritin adsorbed on the BLG surface (Figure 1B). The significant features in the Raman spectra of BLG are the sharp peaks at 1582 cm^{-1} which corresponds to the first-order Raman scattering (called the G band), the second-order peaks involving two (acoustic or optic) phonons (called G' or 2D band) at 2687 cm^{-1} and the peak at 2449 cm^{-1} (called a G*band) is associated with one optical and one acoustic phonon. A second-order peak about half of the frequency of the 2D band at $\sim 1200 \text{ cm}^{-1}$ is called disorder-induced D-band involving one phonon and one defect in the case of CVD graphene which can sometimes be seen in experiments. The observed full width at half maximum (FWHM) of the 2D peak ($\sim 51 \text{ cm}^{-1}$) verifies that our devices consist of BLG. The observed G peak position at 1582 cm^{-1} indicates that the pristine BLG is p-type doped before adsorption of ferritin due to its interaction with the SiO₂ surface (Phillipson et al., 2016; Solís-Fernández et al., 2016). The ratio between intensities of the 2D and G peaks (I_{2D}/I_G) for pristine BLG, densely packed AfFtnAA, and apo-AfFtnAA on BLG

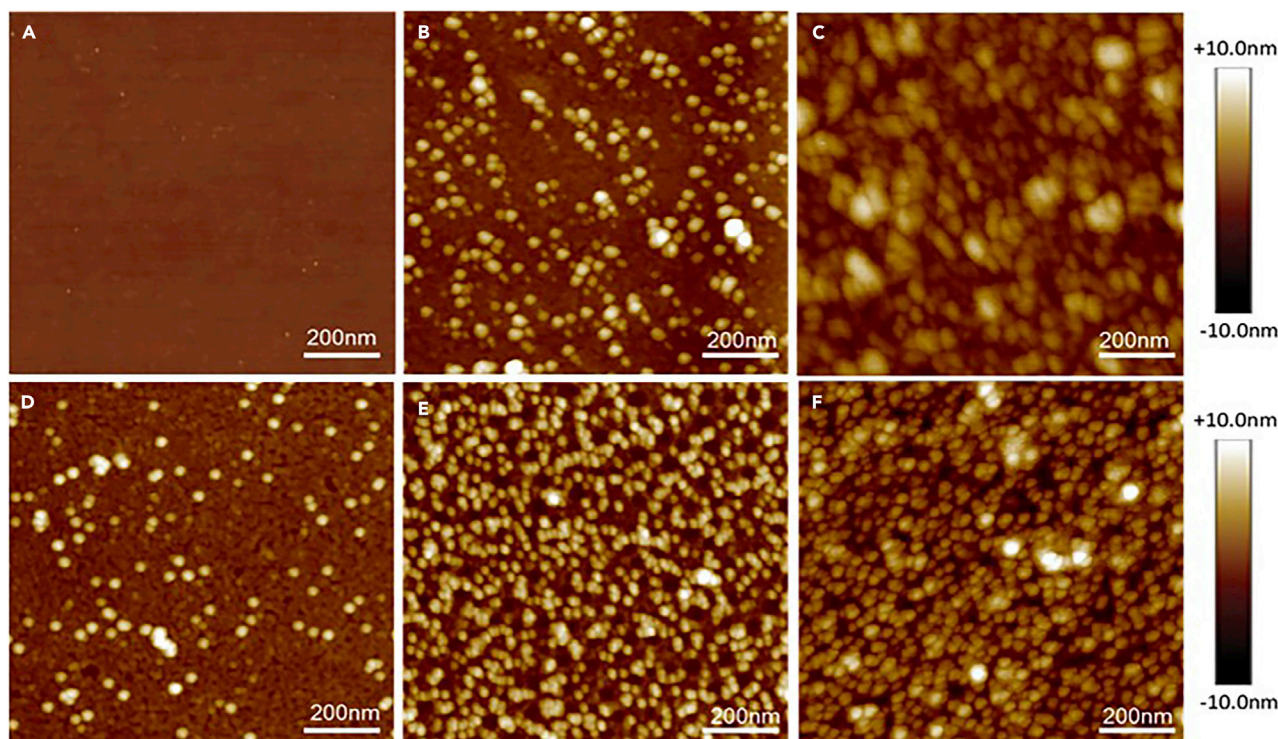


Figure 2. Characterization of ferritin on graphene

(A–F) AFM images of (A) native BLG, and BLG after adsorption of AfFtnAA for 30 min (apoF_{30 min}) (B), or (C) 60 min adsorption (apoF_{60 min}), (D) or adsorption of apo-AfFtnAA for 30 min (F_{30 min}), (E) 60 min adsorption (F_{60 min}), or (F) 120 min (F_{120 min}).

(sample F3 and AF3) is 0.78, 0.81, and 0.95, respectively. This increase in the I_{2D}/I_G ratio is indicative of the adsorption of the biomolecules on BLG which, in turn, results in doping of the BLG (Phillipson et al., 2016; Solís-Fernández et al., 2016). The blue shift in the position of the G peak of 15 cm^{-1} corresponds to a Fermi level (E_F) shift of the graphene of $+0.35\text{ eV}$ (estimated as described in ref (Chen et al., 2011), G peak shift $\Delta\Omega_G = |E_F| \times 42\text{ cm}^{-1}\text{ eV}^{-1}$) upon adsorption of apo-AfFtnAA adsorbed compound which indicates that the molecules interact strongly with the graphene surface. This strong interaction causes charge transfer between apo-AfFtnAA and BLG resulting in n-type doping of BLG. The observed blue shift of the G peak for samples decorated with apo-AfFtnAA consistent with electron-phonon coupling (Das et al., 2009; Manna and Pati, 2009; Crowther et al., 2012) of the adsorption of AfFtnAA (Fe3600 loading/cage) on BLG leads to a red shift of 13 cm^{-1} corresponding to a E_F shift of BLG of -0.30 eV which indicates that AfFtnAA interacts strongly with resulting in p-type doping. It is worth noting that the D peak (peak around $\sim 1200\text{ cm}^{-1}$ corresponding to defect in graphene) does not appear during the exposure of graphene to ferritin even at a highly packed ferritin molecular layer. From these measurements, we conclude that ferritin readily adsorbs on the BLG surface preserving the sp^2 hybridization bond character of graphene, leading to the defect-free formation of a ferritin-graphene heterostructure.

Ferritin—BLG characterization

Figure 2 shows the atomic force microscopy (AFM) images of BLG before and after adsorption of 3000Fe/cage-loaded AfFtnAA and apo-AfFtnAA at different time intervals of 30, 60, and 120 min; hereafter, we define samples F_{30 min}, F_{60 min}, and F_{120 min} as a 30, 60, and 120 min adsorption of ferritin, respectively, similarly apo-AfFtnAA at different adsorption defined as apoF_{30 min} and apoF_{60 min}. Figure 2A shows the AFM image of pristine BLG and Figure 2B shows that a deposition time of 30 min yields isolated AfFtnAA on the surface. Figures 2B–2D shows that a deposition time of 30 min yields isolated apo-AfFtnAA and AfFtnAA on the surface, respectively. Upon increasing the adsorption time to 60 min, the apo-AfFtnAA reaches full monolayer coverage on the BLG surface (Figure 2C) whereas in the case of AfFtnAA, a full monolayer was obtained after 120 min adsorption time (Figure 2F). This adsorption time difference is due to the difference in the size of the apo-AfFtnAA and AfFtnAA on the BLG surface. The height profile (Figure S4)

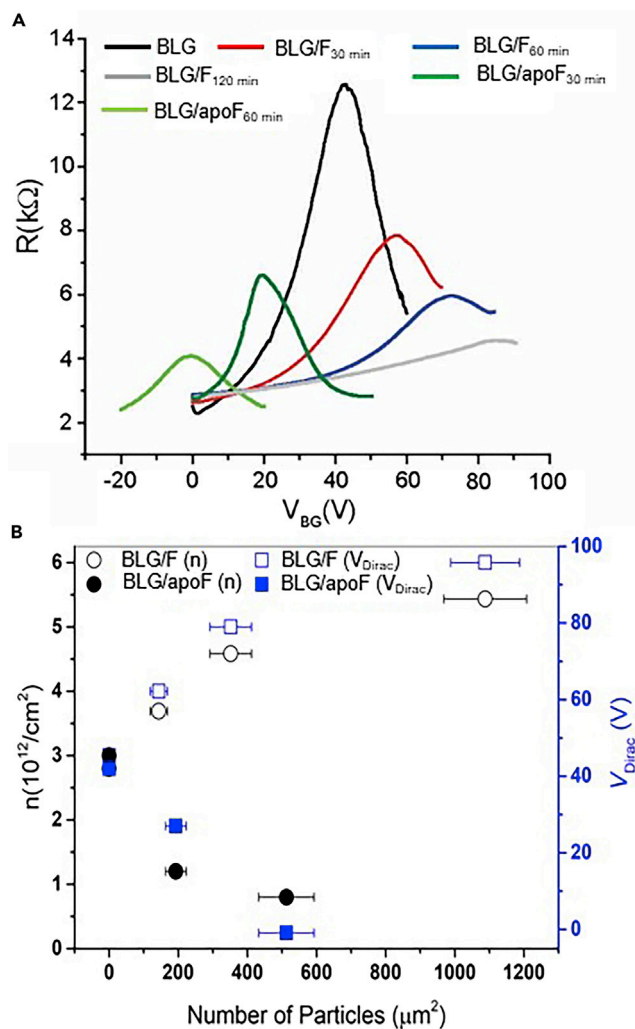


Figure 3. Electrical characteristics as function of ferritin adsorption

(A) Resistance vs gate voltage (R - V_{BG}) curves for a graphene device as fabricated (black line), after adsorption of AfFtnAA (Fe3600/cage) (F) with different adsorption times of 30 min ($F_{30\text{ min}}$), 60 min ($F_{60\text{ min}}$), 120 min ($F_{120\text{ min}}$), and apo- AfFtnAA (apoF) with different adsorption times of 30 min ($apoF_{30\text{ min}}$) and 60 min ($apoF_{60\text{ min}}$). Measurements were performed at a constant voltage bias of 10 mV.

(B) V_{Dirac} -peak position and induced charge carrier density as function of adsorbed number of particles measured by AFM image.

shows that the measured height is 7.0 ± 0.5 nm, which is reasonably close to the outer diameter (12 nm) of AfFtnAA in solution although flattening of AfFtnAA upon adsorption is expected. The height distributions of 3.5 ± 0.5 nm for apo-AfFtnAA and 7.0 ± 0.5 nm of AfFtnAA (Figure S5) are in close agreement with those obtained for apo-AAfFtnAA and AfFtnAA (Fe3600/cage) immobilized via a linker molecule on Au surfaces reported previously (Kumar et al., 2016). For the sake of completion, we also demonstrate that we can obtain dense monolayers by direct adsorption on graphene using a deposition time of 60 min (Figure 2E) or 120 min (Figures 2C and 2F).

Electrical transport characteristics of ferritin-doped BLF-FETs

We determined the charge neutrality point or Dirac point (V_{Dirac}) of the BLG with and without AfFtnAA (Fe3600/cage) adsorbed at different time intervals by measuring the location of the maximum resistance as a function of back-gate voltage (V_{BG}) at room temperature. Figures S2 and S3 show the $I(V)$ and R - V_{BG} curves which were used to construct the R - V_{BG} in Figure 3A. The $I(V)$ shows the linear characteristics of the BLG as a function of applied bias. Figure 3A shows the V_{Dirac} of BLG at $V_{BG} = 40$ V and that the V_{Dirac}

Table 1. Electronic transport characteristics of BLG, BLG/ferritin BLG/apoferritin

| Sample | V_{Dirac} -peak (V) | Shift in the V_{Dirac} -peak (V) | Average induced carrier density ($\times 10^{12} \text{ cm}^{-2}$) | ^a Number of ferritin molecules ($\times 10^{12} \text{ cm}^{-2}$) | Charge induced per ferritin molecule | carrier density/molecule ($\times 10^{12} \text{ cm}^{-2}$) |
|---------------------------|------------------------------|---|--|--|--------------------------------------|---|
| BLG | 42.0 | 0.0 | 0 | 0 | 0 | 0 |
| BLG/F _{30min} | 57.0 | 15.0 | 1.1 | 0.009 | 122 | 113 |
| BLG/F _{60min} | 72.4 | 30.4 | 2.1 | 0.030 | 70 | 65 |
| BLG/F _{120min} | 86.3 | 44.3 | 3.1 | 0.048 | 65 | 60 |
| BLG/apoF _{30min} | 27.0 | -15.0 | -1.1 | 0.014 | -78 | -72 |
| BLG/apoF _{60min} | -0.9 | -41.1 | -2.9 | 0.046 | -63 | -58 |

^aNumber of AfFnAA on the graphene surface determined from the AFM images (Figure 2).

shifts toward more positive values of V_{BG} with increasing adsorption time. It reaches $V_{\text{BG}} = 80 \text{ V}$ after 120 min adsorption indicating p-type doping in exfoliated BLG. Interestingly, in the case of apo-AfFnAA, V_{Dirac} shifts toward negative voltages with $V_{\text{BG}} = -0.9 \text{ V}$ after 60 min adsorption, indicating n-doping. Figure 3B shows that the V_{Dirac} shifts linearly with increasing surface coverage of the ferritin and apoferritin (Figure 3B). These observations suggest that we can control the average doping level by changing the ferritin concentration on the BLG surface and control whether we have electron or hole doping. We would like to point out that ferritin is globular and therefore the protein's orientation does not affect the Dirac peak position.

The changes in charge carrier density (Δn) BLG were estimated by using Equation 1,

$$\Delta n = C_g(V_{\text{BG}} - V_{\text{Dirac}})/e \quad (\text{Equation 1})$$

where C_g is the gate capacitance $\sim 115 \text{ aF } \mu\text{m}^{-2}$ for our Si/SiO₂ substrate, V_{Dirac} is the charge neutrality point of BLG, V_{BG} is the back gate voltage, and e is the electron charge. We can also estimate the induced charge per molecule by utilizing the density of adsorbed molecules as measured from AFM images. The induced charge per molecule changes from 79 ± 23 electrons for AfFnAA and 65 ± 7 (error represent the standard deviation of the surface coverage) holes for apo-AfFnAA (Table 1) based on the surface coverage of the ferritin molecules where the error represents the standard deviation in the surface coverage. The corresponding charge carrier densities per molecule reaches up to 10^{14} cm^{-2} , similar to what is achieved with ionic gating (Yuan et al., 2009). The local charge density for AfFnAA might even be higher because our estimates are derived from the average shift of the V_{Dirac} , which underestimates the actual local charge density induced by individual AfFnAA molecule because of Coulomb repulsion between neighboring molecules. Based on the estimated number of AfFnAA on the BLG (see Section S4 for estimation of ferritin surface coverage) for longer adsorption times of 120 min, we expected the shift in the V_{Dirac} peak position to be around 3.5 times higher than that of the BLG/F_{60 min}. We interpret the 3.5 times lower charge density per molecule at higher coverage as a result of Coulomb repulsion between neighboring molecules. Indeed, the charging mechanism of the molecules in proximity to graphene is interesting by itself. To investigate this in more detail, we conducted electrical transport experiments at low temperatures.

Figure 4 shows the resistance of BLG as a function of back-gate voltage with pristine BLG and with BLG covered with AfFnAA (Fe3600/cage) adsorbed at different durations (BLG/F_{30min} and BLG/F_{60min}) at $T = 1.4 \text{ K}$. As expected, the observed resistance peak remains unchanged for pristine bilayer: only the peak resistance increased at low temperature without significant hysteretic behavior. In contrast, samples with ferritin are strongly hysteretic at low temperatures. Interestingly, these devices show two Dirac peaks for low ferritin coverages. This observation indicates that the observed new peak at 5 V is due to the partial coverage of ferritin induced by local charge transfer on the BLG top-surface, and the peak at high voltage is due to undoped BLG. It is important to note that the observed two Dirac peaks confirm that charge conferment induced by ferritin on the BLG opens up a bandgap in a non-destructive way.

The appearance of hysteresis at low temperature is surprising since conventional hysteresis caused by charge creep (which is effect of the surface charge density on the creep of electrode interface) or charge trapping (which is originated from charge transfer from neighboring adsorbates (such as a water molecule)

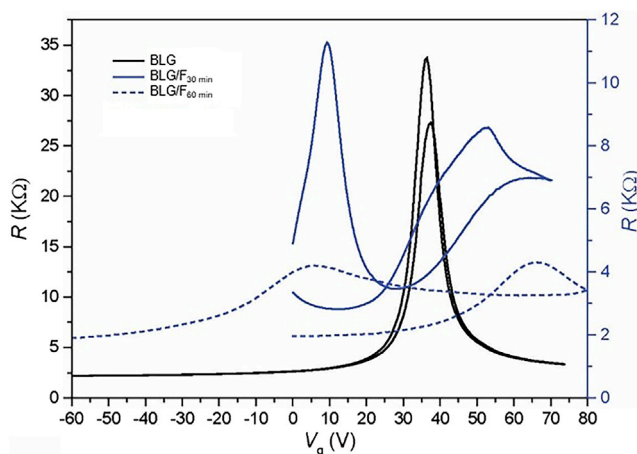


Figure 4. Charge confinement and local gating

Resistance vs gate voltage (R - V_{BG}) curves for a BLG device as fabricated (black line), and after 30 min ($F_{30 \text{ min}}$) and 60 min ($F_{60 \text{ min}}$) adsorption of AfTnAA (Fe3600/cage). Measurements were performed at a constant source-drain voltage bias of 10 mV at 1.4 K.

or charge injection into the trap sites on the dielectric substrate) at the interfaces is usually frozen out at low temperature or at measurements under vacuum conditions (Lohmann et al., 2009; Wang et al., 2010). Here, it seems that charge creep (to and from molecules) is still active at low temperature, implying that charge transfer between molecules and graphene during gate sweeps is too fast to be observed at room temperature.

The presence of the two V_{Dirac} peaks is rare in graphene with self-organized biomolecules. Mulyana et al. also reported two peaks for ferritin adsorbed on a graphene surface, but here the peak modulation was obtained by e-beam irradiation of horse spleen ferritin (Mulyana et al., 2016b). The authors argued that the observed two V_{Dirac} peaks attributed to a certain amount of ferritins which were not completely charged by e-beam irradiation because the e-beam could not penetrate the hydrated iron oxide. We note that it is doubtful that biomolecules can withstand e-beam radiation as radiolysis is well known to occur (Jonge et al., 2009). The gate-voltage tunable V_{Dirac} peak shift and hysteresis have been reported before by controlled adsorption of organic molecules at ambient conditions (Solís-Fernández et al., 2016); however, the distribution of the adsorbed organic molecule is often inhomogeneous, resulting in uncontrolled doping, carrier density variations, and degraded carrier mobility.

CONCLUSIONS

We investigated the electronic characteristics of BLG as a function of the adsorbed ferritin. A highly localized charge state on the graphene surface was created by the highly charged ferritin. Moreover, the structure of BLG was not altered by the adsorption of ferritin due to the noncovalent nature of the interactions between ferritin and BLG. Two-terminal differential resistance traces for BLG with and without ferritin measured at 1.4 K as function of source-drain bias and back-gate voltage, confirm the local charge trapping, and gating, induced by ferritin. This remarkable local charge trapping at ~ 12 nm is promising for future quantum confinement experiments because nanofabrication approaches are difficult to implement and the observation of charge confinement of Dirac electrons in nanostructured graphene is below 100 nm. Our results indicate that ferritin on BLG is an interesting system from both scientific and application point of views, and we hope that our results will stimulate further investigations involving, e.g., spatially resolved methods (STM of c-AFM) or *in situ* spectroscopy measurements.

Limitations of the study

We only used ferritins of one loading quantity (i.e., Fe3600), and it would be interesting to study ferritins at higher and lower loadings. We also only focussed on iron oxide, but ferritins can be loaded with other materials which could lead to improved control of local gating.

STAR★METHODS

Detailed methods are provided in the online version of this paper and include the following:

- **KEY RESOURCES TABLE**
- **RESOURCE AVAILABILITY**
 - Lead contact
 - Data and code availability
- **METHOD DETAILS**
 - General information
 - Ferritin production and purification
 - Atomic force microscopy (AFM)
 - BLG-FET fabrication
 - Formation of ferritin monolayer on BLG-FET
 - Characterization of the monolayers of AfFtn-AA on BLG
 - Electrical measurements of BLG based FET device
 - Extraction of contact resistance

SUPPLEMENTAL INFORMATION

Supplemental information can be found online at <https://doi.org/10.1016/j.isci.2022.104128>.

ACKNOWLEDGMENTS

We acknowledge the Singapore Ministry of Education (MOE) for supporting this research under award No. MOE2015-T2-2-134. The Prime Minister's Office, Singapore, under its Medium-sized Centre program, is also acknowledged for supporting this research.

AUTHOR CONTRIBUTIONS

C.A.N. and J.M. designed and oversaw the project. S.K.K. fabricated the devices and characterized the surfaces. R.R.P. and S.L. prepared the proteins. S.K.K. and W.X. carried out the electrical measurements. All authors wrote and commented on the manuscript.

DECLARATION OF INTERESTS

Christian A. Nijhuis is an Editorial advisory board member of iScience.

Received: October 27, 2021

Revised: January 11, 2022

Accepted: March 17, 2022

Published: April 15, 2022

REFERENCES

- Allen, M.T., Martin, J., and Yacoby, A. (2012). Gate-defined quantum confinement in suspended bilayer graphene. *Nat. Commun.* **3**, 934. <https://doi.org/10.1038/ncomms1945>.
- Brenner, K., and Murali, R. (2010). Single step, complementary doping of graphene. *Appl. Phys. Lett.* **96**, 063104. <https://doi.org/10.1063/1.3308482>.
- Cavalleri, O., Natale, C., Stroppolo, M.E., Relini, A., Cosulich, E., Thea, S., and Gliozzi, A. (2000). Azurin immobilisation on thiol covered Au(111). *Phys. Chem. Chem. Phys.* **2**, 4630–4635. <https://doi.org/10.1039/b003603j>.
- Chen, C.F., Park, C.H., Boudouris, B.W., Horng, J., Geng, B., Girit, C., Zettl, A., Crommie, M.F., Segalman, R.A., Louie, S.G., and Wang, F. (2011). Controlling inelastic light scattering quantum pathways in graphene. *Nature* **471**, 617–620. <https://doi.org/10.1038/nature09866>.
- Chiu, H.-Y., Perebeinos, V., Lin, Y.M., and Avouris, P. (2010). Controllable p-n junction formation in monolayer graphene using electrostatic substrate engineering. *Nano Lett.* **10**, 4634–4639. <https://doi.org/10.1021/nl102756r>.
- Crowther, A.C., Ghassaei, A., Jung, N., and Brus, L.E. (2012). Strong charge-transfer doping of 1 to 10 layer graphene by NO₂. *ACS Nano* **6**, 1865–1875. <https://doi.org/10.1021/nn300252a>.
- Das, A., Chakraborty, B., Piscanec, S., Pisana, S., Sood, A.K., and Ferrari, A.C. (2009). Phonon renormalization in doped bilayer graphene. *Phys. Rev. B* **79**, 155417. <https://doi.org/10.1103/PhysRevB.79.155417>.
- Dong, X., Fu, D., Fang, W., Shi, Y., Chen, P., and Li, L.J. (2009). Doping single-layer graphene with aromatic molecules. *Small*, 1422–1426. <https://doi.org/10.1002/smll.200801711>.
- Dubey, S., Singh, V., Bhat, A.K., Parikh, P., Grover, S., Sensarma, R., Tripathi, V., Sengupta, K., and Deshmukh, M.M. (2013). Tunable superlattice in graphene to control the number of dirac points. *Nano Lett.* **13**, 3990–3995. <https://doi.org/10.1021/nl4006029>.
- Farmer, D.B., Lin, Y.M., Afzali-Ardakani, A., and Avouris, P. (2009). Behavior of a chemically doped graphene junction. *Appl. Phys. Lett.* **94**, 213106. <https://doi.org/10.1063/1.3142865>.
- Fehske, H., Hager, G., and Pieper, A. (2015). Electron confinement in graphene with gate-defined quantum dots. *Phys. Status Solidi B* **252**, 1868–1871. <https://doi.org/10.1002/pssb.201552119>.
- Frasconi, M., Mazzei, F., and Ferri, T. (2010). Protein immobilization at gold-thiol surfaces and potential for biosensing. *Anal. Bioanal. Chem.*

- 398, 1545–1564. <https://doi.org/10.1007/s00216-010-3708-6>.
- Gorbachev, R.V., Song, J.C., Yu, G.L., Kretinin, A.V., Withers, F., Cao, Y., Mishchenko, A., Grigorieva, I.V., Novoselov, K.S., Levitov, L.S., and Geim, A.K. (2014). Detecting topological currents in graphene superlattices. *Science* 346, 448–451. <https://doi.org/10.1126/science.1254966>.
- Hong, L., Nishihara, T., Hijikata, Y., Miyauchi, Y., and Itami, K. (2018). Unidirectional molecular assembly alignment on graphene enabled by nanomechanical symmetry breaking. *Sci. Rep.* 8, 1–8. <https://doi.org/10.1038/s41598-018-20760-z>.
- de Jonge, N., Peckys, D.B., Kremers, G.J., and Piston, D.W. (2009). Electron microscopy of whole cells in liquid with nanometer resolution. *Proc. Natl. Acad. Sci. U S A* 106, 2159–2164. <https://doi.org/10.1073/pnas.0809567106>.
- Joshi, P., Romero, H.E., Neal, A.T., Toutam, V.K., and Tadigadapa, S.A. (2010). Intrinsic doping and gate hysteresis in graphene field effect devices fabricated on SiO₂ substrates. *J. Phys. Condensed Matter* 22, 334214. <https://doi.org/10.1088/0953-8984/22/33/334214>.
- Katsnelson, M.I., Novoselov, K.S., and Geim, A.K. (2006). Chiral tunnelling and the Klein paradox in graphene. *Nat. Phys.* 2, 620–625. <https://doi.org/10.1038/nphys384>.
- Kim, J.W., Choi, S.H., Lillehei, P.T., Chu, S.H., King, G.C., and Watt, G.D. (2007). Electrochemically controlled reconstitution of immobilized ferritins for bioelectronic applications. *J. Electroanal. Chem.* 601, 8–16. <https://doi.org/10.1016/j.jelechem.2006.10.018>.
- Kim, Y.D., Bae, M.H., Seo, J.T., Kim, Y.S., Kim, H., Lee, J.H., Ahn, J.R., Lee, S.W., Chun, S.H., and Park, Y.D. (2013). Focused-laser-enabled p–n junctions in graphene field-effect transistors. *ACS Nano* 7, 5850–5857. <https://doi.org/10.1021/nn402354j>.
- Kong, L., Enders, A., Rahman, T.S., and Dowben, P.A. (2014). Molecular adsorption on graphene. *J. Phys. Condensed Matter* 26, 443001. <https://doi.org/10.1088/0953-8984/26/44/443001>.
- Krishna Kumar, R., Chen, X., Auton, G.H., Mishchenko, A., Bandurin, D.A., Morozov, S.V., Cao, Y., Khestanova, E., Ben Shalom, M., Kretinin, A.V., et al. (2017). High-temperature quantum oscillations caused by recurring Bloch states in graphene superlattices. *Science* 357, 181–184. <https://doi.org/10.1126/science.aal3357>.
- Kulkarni, G.S., Reddy, K., Zang, W., Lee, K., Fan, X., and Zhong, Z. (2016). Electrical probing and tuning of molecular physisorption on graphene. *Nano Lett.* 16, 695–700. <https://doi.org/10.1021/acs.nanolett.5b04500>.
- Kumar, K.S., Pasula, R.R., Lim, S., and Nijhuis, C.A. (2016). Long-range tunneling processes across ferritin-based junctions. *Adv. Mater.* 28, 1824–1830. <https://doi.org/10.1002/adma.201504402>.
- Lin, H., Fratesi, G., and Brivio, G.P. (2015). Graphene magnetism induced by covalent adsorption of aromatic radicals. *Phys. Chem. Chem. Phys.* 17, 2210–2215. <https://doi.org/10.1039/c4cp04476b>.
- Liu, W., Wei, J., Sun, X., and Yu, H. (2013). A study on graphene—metal contact. *Crystals* 3, 257–274. <https://doi.org/10.3390/cryst3010257>.
- Liu, X., Jin, W., and Theil, E.C. (2003). Opening protein pores with chaotropes enhances Fe reduction and chelation of Fe from the ferritin biomineral. *Proc. Natl. Acad. Sci. U S A* 100, 3653–3658. <https://doi.org/10.1073/pnas.0636928100>.
- Logemann, R., Reijnders, K.J.A., Tudorovskiy, T., Katsnelson, M.I., and Yuan, S. (2015). Modeling Klein tunneling and caustics of electron waves in graphene. *Phys. Rev. B* 91, 045420. <https://doi.org/10.1103/PhysRevB.91.045420>.
- Lohmann, T., von Klitzing, K., and Smet, J.H. (2009). Four-terminal magneto-transport in graphene p–n junctions created by spatially selective doping. *Nano Lett.* 9, 1973–1979. <https://doi.org/10.1021/nl900203n>.
- Macleod, J.M., and Rosei, F. (2014). Molecular self-assembly on graphene. *Small* 10, 1038–1049. <https://doi.org/10.1002/smll.201301982>.
- Manna, A.K., and Pati, S.K. (2009). Tuning the electronic structure of graphene by molecular charge transfer: a computational study. *Chem. Asian J.* 4, 855–860. <https://doi.org/10.1002/asia.200800486>.
- Mojarad, N., Hojeij, M., Wang, L., Gobrecht, J., and Ekcinci, Y. (2015). Single-digit-resolution nanopatterning with extreme ultraviolet light for the 2.5 nm technology node and beyond. *Nanoscale* 7, 4031–4037. <https://doi.org/10.1039/C4NR07420C>.
- Mulyana, Y., Uenuma, M., Okamoto, N., Ishikawa, Y., Yamashita, I., and Uraoka, Y. (2016a). Creating reversible p–n junction on graphene through ferritin adsorption. *ACS Appl. Mater. Inter.* 8, 8192–8200. <https://doi.org/10.1021/acsmi.5b12226>.
- Mulyana, Y., Uenuma, M., Okamoto, N., Ishikawa, Y., Yamashita, I., and Uraoka, Y. (2016b). Creating reversible p–n junction on graphene through ferritin adsorption. *ACS Appl. Mater. Inter.* 8, 8192–8200. <https://doi.org/10.1021/acsmi.5b12226>.
- Novoselov, K.S., Geim, A.K., Morozov, S.V., Jiang, D., Zhang, Y., Dubonos, S.V., Grigorieva, I.V., and Firsov, A.A. (2004). Electric field effect in atomically thin carbon films. *Science* 306, 666–669. <https://doi.org/10.1126/science.1102896>.
- Oh, H., Coh, S., Son, Y.W., and Cohen, M.L. (2016). Inhibiting Klein tunneling in a graphene p–n junction without an external magnetic field. *Phys. Rev. Lett.* 117, 016804. <https://doi.org/10.1103/PhysRevLett.117.016804>.
- Overweg, H., Eggimann, H., Chen, X., Slizovskiy, S., Eich, M., Pisoni, R., Lee, Y., Rickhaus, P., Watanabe, K., Taniguchi, T., and Fal'ko, V. (2018). Electrostatically induced quantum point contacts in bilayer graphene. *Nano Lett.* 18, 553–559. <https://doi.org/10.1021/acs.nanolett.7b04666>.
- Papamatthaiou, S., Estrela, P., and Moschou, D. (2021). Printable graphene BioFETs for DNA quantification in Lab-on-PCB microsystems. *Sci. Rep.* 11, 9815. <https://doi.org/10.1038/s41598-021-89367-1>.
- Park, J., Jo, S.B., Yu, Y.J., Kim, Y., Yang, J.W., Lee, W.H., Kim, H.H., Hong, B.H., Kim, P., Cho, K., and Kim, K.S. (2012). Single-gate bandgap opening of bilayer graphene by dual molecular doping. *Adv. Mater.* 24, 407–411. <https://doi.org/10.1002/adma.201103411>.
- Phillipson, R., Lockhart de la Rosa, C.J., Teyssandier, J., Walke, P., Waghray, D., Fujita, Y., Adisojoso, J., Mali, K.S., Asselberghs, I., Huyghebaert, C., and Uji-I, H. (2016). Tunable doping of graphene by using physisorbed self-assembled networks. *Nanoscale* 8, 20017–20026. <https://doi.org/10.1039/c6nr07912a>.
- Qiu, H., Dong, X., Sana, B., Peng, T., Paramelle, D., Chen, P., and Lim, S. (2013). Ferritin-templated synthesis and self-assembly of Pt nanoparticles on a monolithic porous graphene network for electrocatalysis in fuel cells. *ACS Appl. Mater. Interfaces* 5, 782–787.
- Samuels, A.J., and Carey, J.D. (2013). Molecular doping and band-gap opening of bilayer graphene. *ACS Nano* 7, 2790–2799. <https://doi.org/10.1021/nn400340q>.
- San, B.H., Kim, J.A., Kulkarni, A., Moh, S.H., Dugasani, S.R., Subramani, V.K., Thorat, N.D., Lee, H.H., Park, S.H., Kim, T., and Kim, K.K. (2014). Combining protein-shelled platinum nanoparticles with graphene to build a bionanohybrid capacitor. *ACS Nano* 8, 12120–12129. <https://doi.org/10.1021/nn503178t>.
- Sana, B., Johnson, E., Sheah, K., Poh, C.L., and Lim, S. (2010). Iron-based ferritin nanocore as a contrast agent. *Biointerphases* 5, FA48. <https://doi.org/10.1116/1.3483216>.
- Sana, B., Johnson, E., Le Magueres, P., Criswell, A., Cascio, D., and Lim, S. (2013). The role of nonconserved residues of Archaeoglobus fulgidus ferritin on its unique structure and biophysical properties. *J. Biol. Chem.* 288, 32663–32672. <https://doi.org/10.1074/jbc.M113.491191>.
- Seo, B.H., Youn, J., and Shim, M. (2014). Direct laser writing of air-stable p–n junctions in graphene. *ACS Nano* 8, 8831–8836. <https://doi.org/10.1021/nn503574p>.
- Solís-Fernández, P., Okada, S., Sato, T., Tsuji, M., and Ago, H. (2016). Gate-tunable dirac point of molecular doped graphene. *ACS Nano* 10, 2930–2939. <https://doi.org/10.1021/acsnano.6b00064>.
- Solnyshkov, D., Nalitov, A., Teklu, B., Franck, L., and Malpuech, G. (2016). Spin-dependent Klein tunneling in polariton graphene with photonic spin-orbit interaction. *Phys. Rev. B* 93, 085404. <https://doi.org/10.1103/PhysRevB.93.085404>.
- Song, P., Sangeeth, C.S.S., Thompson, D., Du, W., Loh, K.P., and Nijhuis, C.A. (2016). Noncovalent self-assembled monolayers on graphene as a highly stable platform for molecular tunnel junctions. *Adv. Mater.* 28, 631–639. <https://doi.org/10.1002/adma.201504207>.
- Sun, J., Muruganathan, M., and Mizuta, H. (2016). Room temperature detection of individual molecular physisorption using suspended bilayer graphene. *Sci. Adv.* 2, e1501518. <https://doi.org/10.1126/sciadv.1501518>.
- Tran, T.-T., and Mulchandani, A. (2016). Carbon nanotubes and graphene nano field-effect

- transistor-based biosensors. *Trac Trends Anal. Chem.* **79**, 222–232. <https://doi.org/10.1016/j.trac.2015.12.002>.
- Trauzettel, B., Bulaev, D.V., Loss, D., and Burkard, G. (2007). Spin qubits in graphene quantum dots. *Nat. Phys.* **3**, 192–196. <https://doi.org/10.1038/nphys544>.
- Velasco, J., Lee, J., Wong, D., Kahn, S., Tsai, H.Z., Costello, J., Crommie, M.F., et al. (2018). Visualization and control of single-electron charging in bilayer graphene quantum dots. *Nano Lett.* **18**, 5104–5110. <https://doi.org/10.1021/acs.nanolett.8b01972>.
- Vicarelli, L., Heerema, S.J., Dekker, C., and Zandbergen, H.W. (2015). Controlling defects in graphene for optimizing the electrical properties of graphene nanodevices. *ACS Nano* **9**, 3428–3435. <https://doi.org/10.1021/acs.nano.5b01762>.
- Wang, H., Wu, Y., Cong, C., Shang, J., and Yu, T. (2010). Hysteresis of electronic transport in graphene transistors. *ACS Nano* **4**, 7221–7228. <https://doi.org/10.1021/nn101950n>.
- Watt, G.D., Kim, J.W., Zhang, B., Miller, T., Harb, J.N., Davis, R.C., and Choi, S.H. (2012). A protein-based ferritin bio-nanobattery. *J. Nanotechnol.* **2012**, 1–9. <https://doi.org/10.1155/2012/516309>.
- Winter, A., Ekinci, Y., Götzhäuser, A., and Turchanin, A. (2019). Freestanding carbon nanomembranes and graphene monolayers nanopatterned via EUV interference lithography. *2D Mater* **6**, 021002. <https://doi.org/10.1088/2053-1583/ab0014>.
- Won, K., Park, M.J., Yoon, H.H., and Kim, J.H. (2008). Immobilization of iron storage protein on a gold electrode based on self-assembled monolayers. *Ultramicroscopy* **108**, 1342–1347. <https://doi.org/10.1016/j.ultramicro.2008.04.088>.
- Xiao, K., Deng, W., Keum, J.K., Yoon, M., Vlassiok, I.V., Clark, K.W., and Geoghegan, D.B. (2013). Surface-induced orientation control of CuPc molecules for the epitaxial growth of highly ordered organic crystals on graphene. *J. Am. Chem. Soc.* **135**, 3680–3687. <https://doi.org/10.1021/ja3125096>.
- Yang, Y., and Wang, C. (2009). Solvent effects on two-dimensional molecular self-assemblies investigated by using scanning tunneling microscopy. *Curr. Opin. Colloid Interf. Sci.* **14**, 135–147. <https://doi.org/10.1016/j.cocis.2008.10.002>.
- Young, A.F., and Kim, P. (2009). Quantum interference and Klein tunnelling in graphene heterojunctions. *Nat. Phys.* **5**, 222–226. <https://doi.org/10.1038/nphys1198>.
- Yuan, D., Ding, L., Chu, H., Feng, Y., McNicholas, T.P., and Liu, J. (2008). Horizontally aligned single-walled carbon nanotube on quartz from a large variety of metal catalysts. *Nano Lett.* **8**, 2576–2579. <https://doi.org/10.1021/nl801007r>.
- Yuan, H., Shimotani, H., Tsukazaki, A., Ohtomo, A., Kawasaki, M., and Iwasa, Y. (2009). High-density carrier accumulation in ZnO field-effect transistors gated by electric double layers of ionic liquids. *Adv. Funct. Mater.* **19**, 1046–1053. <https://doi.org/10.1002/adfm.200801633>.
- Yun, J.M., Park, S., Hwang, Y.H., Lee, E.S., Maiti, U., Moon, H., and Kim, S.O. (2014). Complementary p- and n-type polymer doping for ambient stable graphene inverter. *ACS Nano* **8**, 650–656. <https://doi.org/10.1021/nn4053099>.
- Zhao, Y., Wyrick, J., Natterer, F.D., Rodriguez-Nieva, J.F., Lewandowski, C., Watanabe, K., and Stroscio, J.A. (2015). Creating and probing electron whispering-gallery modes in graphene. *Science* **348**, 672–675. <https://doi.org/10.1126/science.aaa7469>.

STAR★METHODS

KEY RESOURCES TABLE

| REAGENT or RESOURCE | SOURCE | IDENTIFIER |
|---|---|----------------|
| Chemicals, peptides, and recombinant proteins | | |
| silicon wafers (100, p-type, 0.001 ohm-cm) with 300 nm SiO ₂ deposited and one side polished | University Wafers (USA) | Item No:452 |
| Gold (purity of 99.999%) | Superconductor Material, Inc (USA) | CAS:7440-57-5 |
| Titanium (purity of 99.999%) | Superconductor Material, Inc (USA) | CAS:7440-32-6 |
| ferrous sulfate heptahydrate | Sigma-Aldrich | CAT#7782-63-0 |
| ferrous sulfate solution | | |
| HEPES buffer (25 mM HEPES, 50 mM NaCl, pH 8) | | |
| Hydrochloric acid | Sigma-Aldrich | CAT# 7647-01-0 |
| AfFtn-AA | R&D | PDB ID3KX9 |
| Critical commercial assays | | |
| BCA assay kit | Thermo Fisher Scientific Inc, Rockford, USA | CAT#23225 |
| Amicon centrifugal filters (100 kDa MWCO) | Millipore, Billerica, MA | CAT#ACS510024 |
| Software and algorithms | | |
| LabView | NI Solutions | Version 2010 |
| Origin Pro | Origin Lab | 2019b |
| Other | | |
| Amicon centrifugal filters (100 kDa MWCO) | Millipore, Billerica, MA | CAT#ACS510024 |

RESOURCE AVAILABILITY

Lead contact

Further information and requests for resources and reagents should be directed to and will be fulfilled by the lead contact, C.A. Nijhuis (c.a.nijhuis@utwente.nl).

Data and code availability

Any additional information required to reanalyze the data reported in this paper is available from the lead contact upon request.

METHOD DETAILS

General information

We purchased silicon wafers (100, p-type, 0.001 ohm-cm) with 300 nm SiO₂ deposited and one side polished from University Wafers (USA). We purchased gold (Au) and titanium (Ti) with a purity of 99.999% from Superconductor Material, Inc (USA). The solvents were AR grade.

Ferritin production and purification

The ferritins used in this study were derived from a hyper-thermophilic archaeon *Archaeoglobus fulgidus* (PDB ID 3KX9; AfFtn-AA), which has high thermal stability (up to 80 °C). Ferritins convert aqueous Fe²⁺ into insoluble Fe³⁺ in the form of ferrihydrite nanoparticles. Here, the amount of iron ions inside the ferritin was 3600 Fe (which indicates the molecular ratio of the ferritin with respect to Fe). The ferritin iron composites were prepared via previously reported procedures followed by expression and purification of AfFtn-AA (Sana et al., 2010). Iron loading into ferritin was carried as follows (Liu et al., 2003). Dimeric apoferritin was incubated with freshly prepared ferrous sulfate solution in 0.1% HCl for 1 h at room temperature followed by overnight incubation at 4 °C. Iron loading (3600) was achieved by adding required moles of iron sulfate solution to the dimeric ferritin solution (1 μM ferritin = 500 μg/mL ferritin). Amicon centrifugal filters (100 kDa MWCO; Millipore, Billerica, MA) were used to remove the unbound iron by buffer exchange. Protein quantification was performed using the BCA assay kit (Thermo Fisher Scientific Inc, Rockford, USA).

Atomic force microscopy (AFM)

The AFM images of Si/SiO₂/BLG with and without ferritin monolayers with different adsorption times were obtained with a Bruker Dimension FastScan AFM in tapping mode with FASTSCAN-A tips. AFM software NanoScope Analysis (version 1.4) was used to analyse the AFM images.

BLG-FET fabrication

The BLG film was exfoliated and deposited on a 300 nm SiO₂/p + -Si substrate using the Scotch tape method as described before (Novoselov, 2004). We fabricated the source/drain electrodes through standard methods using e-beam lithography and deposition of Au/Ti (60/5 nm) with a thermal evaporator, followed by lift-off in acetone for 10 min. Before use, we vacuum annealed the devices at 200°C with a heating rate of 1.8°C/s for 2 h at a base pressure of 5×10^{-6} mbar to clean the BLG surface. We characterized the quality of the BLG before and after vacuum annealing using Raman spectroscopy (Figure S6).

Formation of ferritin monolayer on BLG-FET

The ferritin was self-assembled on the BLG surface at different time intervals 30, 60, and 120 min, from a HEPES buffer (25 mM HEPES, 50 mM NaCl, pH 8) solution with a concentration of 1 μM. After adsorption, the BLG-FET was rinsed with deionized water to remove non-specifically bound ferritin. The devices were dried in a stream of N₂ gas. A similar procedure was followed to prepare a monolayer of apoferritin on the BLG surface.

Characterization of the monolayers of AfFtn-AA on BLG

Mostly, ferritin is adsorbed on gold electrodes via modification of ferritins with thiol containing amino acids (cysteine) followed by deposition on Au or by first forming a linker monolayer on Au followed by deposition of ferritin (Kim et al., 2007; Won et al., 2008; Frasconi et al., 2010). Here, we directly adsorbed AfFtn-AA on graphene where AfFtn-AA readily binds to graphene likely via electrostatic interactions (as discussed in the main text) in addition to non-specific interactions (including amines exposed at the periphery that may interact strongly with graphene (Mulyana et al., 2016a, 2016b; Song et al., 2016; Papamatthaiou et al., 2021). Figure S4 shows additional AFM images and the height profiles corresponding to the white lines. The apparent width of AfFtn-AA of 40–60 nm is considerably larger than the true dimension, mainly due to AFM tip broadening (Cavalleri et al., 2000). Most of the observed ferritins in the AFM images are isolated. These results are very close those reported for AfFtn-AA adsorbed on Au surfaces from which we conclude that the ferritins largely retain their globular shape although some flattening occurs depending on the loading (as mentioned in the text and discussed in detail in Song et al., 2016). Figure S5 shows the height distribution of AfFtn-AA, $d_{\text{AfFtn-AA}}$ on BLG determined from such line scans. We determined the surface coverage of the AfFtn-AA by counting all AfFtn-AA visible in the AFM images which have a $1 \times 1 \mu\text{m}^2$ area.

Electrical measurements of BLG based FET device

The electronic properties of the before and after adsorption of ferritin on the BLG were characterized using FETs. The applied gate voltage dependent resist of the BLG measurements were performed with a cryogen-free cryostat (ICEoxford, Lemon System), equipped with 8 T superconducting electromagnet in the range of temperature of 1.37–300 K. We recorded the V_{Dirac} curves using the home-written code in LabView (Version, 2010) and a Keithley 6430 sub-femtoamp remote source meter.

Extraction of contact resistance

To extract the contact and channel resistance of the devices, we fabricated 2-terminals within a single graphene flake with varying channel lengths ranging from 3 to 24 μm. The two-terminal resistance of each device was measured at zero back gate voltage at room temperature. The resistance R of each device is plotted as function of channel length as shown in Figure S1. The data is fitted using the Equation (S1),

$$R = 2R_c(W) + \rho L/W \quad (\text{Equation S1})$$

where R_c is the contact resistance of each contact as a function of width, ρ is the resistivity of the channel, L and W are the channel length and width, respectively. The contact resistance of BLG and BLG/ $F_{60 \text{ min}}$ are 243 and 350 Ω/μm. The observed contact resistance of the fabricated device is similar to that reported for devices with Ti/Au contacts (Liu et al., 2013).